A Time-dependent Creep Model for Salt

D.E. Maxwell, K.K. Wahi, J.E. Reaugh and R. Hofmann

Science Applications Inc.,
2450 Washington Avenue, San Leandro, California 94577

ABSTRACT

A creep model for salt has been developed which, when given constitutive constants derived from laboratory pillar experiments and used in conjunction with an explicit finite-difference code, gives excellent agreement with data from a field test called Project Salt Vault (PSV). The model is a generalized version of the Starfield-McClain creep strain-rate model and allows for varying temperature and stress fields. It incorporates a stress relaxation algorithm developed by Wilkins, based on the non-associative Prandtl-Reuss flow rule. The numerical method solves a set of explicit-in-time physical equations which are represented by explicit finite-difference numerical equations. The coupled constitutive equations are solved using a Runge Kutta scheme. A time-dependent, two-dimensional planestrain simulation of PSV was compared to room convergence data which was gathered at intervals during the 23-month experiment. These data compared remarkably well. This paper contains a discussion of the physical and theoretical basis for the model, as well as a description of the numerical procedure used to integrate the creep formulas.

INTRODUCTION

A creep model for salt has been developed by Science Applications, Inc. (SAI) which, when given constitutive constants derived from laboratory pillar experiments and used in conjunction with an explicit finite-difference code, gives excellent agreement with data from a field test called Project Salt Vault (PSV). The model is a generalized version of the Starfield-McClain (S&M) creep strain-rate model and allows for varying temperature and stress fields. It incorporates a stress relaxation algorithm developed by Wilkins, based on the non-associative Prandtl-Reuss flow rule. The numerical method solves a set of explicit-in-time physical equations which are represented by explicit finite-difference numerical equations. The coupled constitutive equations are solved using a Runge Kutta scheme. A time-dependent, two-dimensional plane-strain simulation of PSV was compared to room convergence data which was gathered at intervals during the 23-month experiment. The computational and experimental data compared remarkably well. This paper contains a discussion of the physical and theoretical basis for the model, as well as a description of the numerical procedure used to integrate the creep formulas.

PHYSICAL AND THEORETICAL BASIS FOR THE MODEL

The laboratory pillar experiments of Lomenick, reported in Reference 1, provided the basis for both the SAI model and the S&M model of Reference 2. The experimental configurations were small-scale mock-ups of cylindrical salt pillars, as shown schematically in the diagrams of Figure 1. The time-dependent strain of the pillar height, defined by the gap distance, x, was obtained for different conditions of temperature and average vertical stress in the pillar. The temperatures ranged from about 20 to 200 degrees Centigrade. The vertical stress ranged from zero to about 4.14×10^7 Pa (6000 psi) and was defined by the ratio of the load to the cross-sectional area of the pillar.

The vertical stress was applied suddenly in all of these experiments and was not varied during a given experiment. It would have been desirable if the stress had been changed while creep was occurring in some of the experiments. This was not done, and assumptions had to be employed to model this feature. The S&M and SAI models employed different assumptions and, consequently, predict different creep responses for stress changes, as will be seen later. Fortunately, the temperature *was* changed while creep was

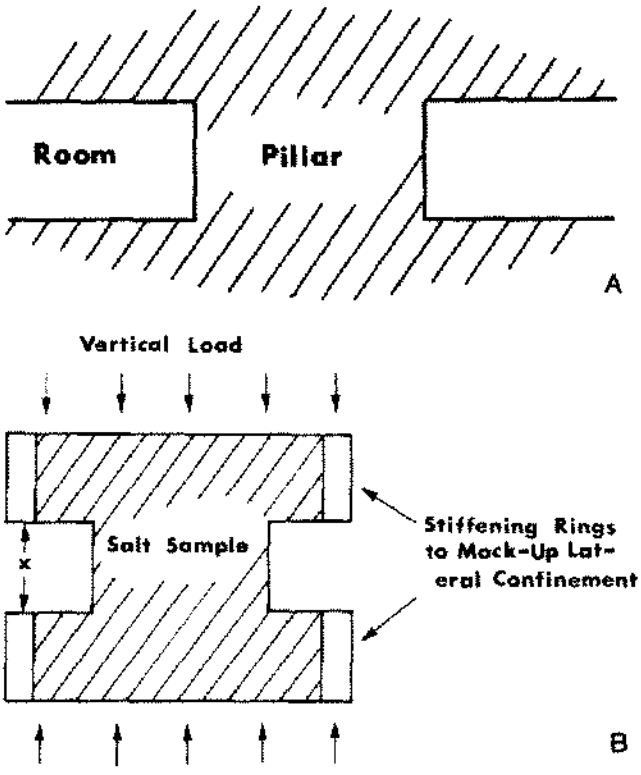

Figure 1. Schematic geometry of small-scale experiments. a) In-situ cylindrical salt pillar. b) small-scale mock-up of pillar region.

occurring in some of these experiments. Consequently, the S&M and SAI models are identical with respect to this feature.

The diagrams of Figure 2 illustrate a case of constant temperature. Figure 2(a) shows the applied conditions. The pillar creep strain, ϵ_x, and creep strain rate, $\dot{\epsilon}_x$, are shown schematically in Figures 2(b) and 2(c), and can be fit by the forms

$$\epsilon_x = A(t-t_0)^a\,\theta^b\sigma_x^c \qquad \text{(A-1a)}$$

$$\dot{\epsilon}_x = a\epsilon_x/(t-t_0) \qquad \text{(A-1b)}$$

where a, b, and c are material constants, while the value of A depends on the geometry as well as on the material; t is time; θ is temperature; and σ_x is the vertical pillar load in stress units.

The diagrams of Figure 3 display a case with a temperature jump at t_1. The observed response can be fit as an overlay of two constant temperature cases with a time shift to provide creep strain continuity at t_1. The creep strain and its rate after t_1 can be fit by the forms

$$\epsilon_x(t>t_1) = A(t-\lambda)^a\theta_1^b\sigma_0^c \qquad \text{(A-2a)}$$

$$\dot{\epsilon}_x(t>t_1) = a\epsilon_x/(t-\lambda) \qquad \text{(A-2b)}$$

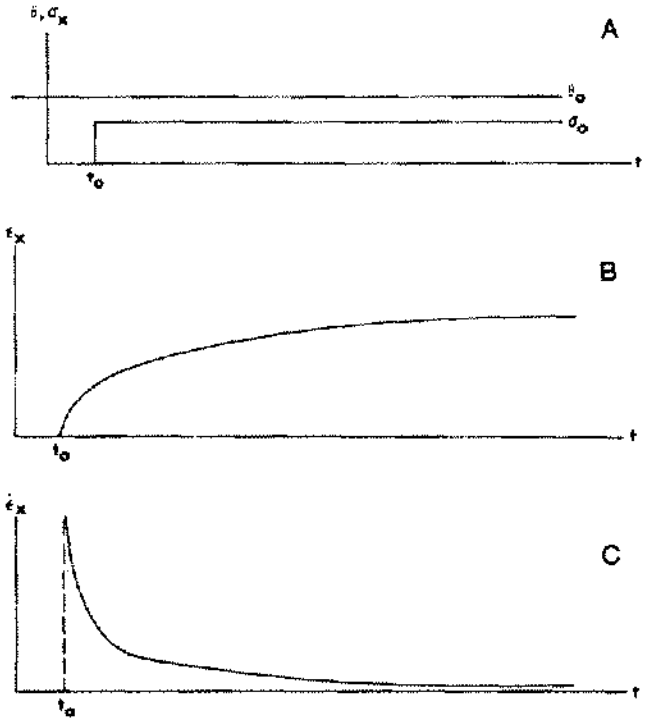

Figure 2. Schematics of constant temperature case. a) Imposed conditions of temperature and stress. b) Creep strain response. c) Creep strain rate response.

where the value of λ provides creep strain continuity at t_1. Hence, λ can be obtained from Eqs. (A-1a) and (A-2a) as follows,

$$(t_1-t_0)^a\theta_0^b\sigma_0^c = (t_1-\lambda)^a\theta_1^b\sigma_0^c.$$

The previous expressions can then be generalized for continuous temperature changes (with constant stress) by the differential expressions

$$d\epsilon_x = \frac{\partial\epsilon_x}{\partial t}\,dt + \left[\frac{\partial\epsilon_x}{\partial\lambda}\,d\lambda + \frac{\partial\epsilon_x}{\partial\theta}\,d\theta\right]$$

$$= \frac{a\epsilon_x}{t-\lambda}\,dt + \left[-\frac{a\epsilon_x\,d\lambda}{t-\lambda} + \frac{b\epsilon_x\,d\theta}{\theta}\right].$$

By definition, a finite change of creep strain requires a finite time interval and the sum of the terms in the bracket is identically zero. Thus, the SAI and S&M pillar models for constantt stress with temperature changes can be expressed as

$$\epsilon_x(\text{const }\sigma_x) = A[t-\lambda(t)]^a\,[\theta(t)]^b\,\sigma_0^c \qquad \text{(A-3a)}$$

$$\dot{\epsilon}_x = a\,\epsilon_x/[t-\lambda(t)] \qquad \text{(A-3b)}$$

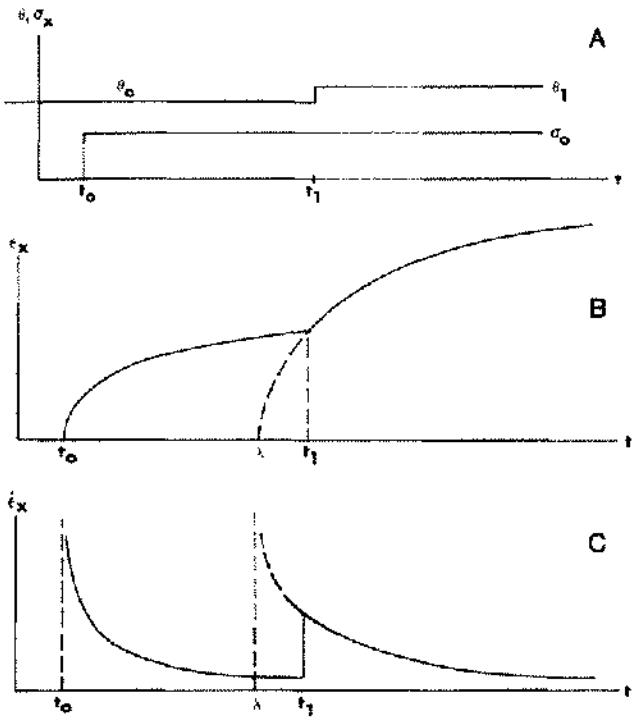

Figure 3. Schematics of temperature jump case. a) Imposed conditions of temperature and stress. b) Creep strain response. c) Creep strain rate response.

where

$$\lambda(\text{const}\,\sigma_x) = \lambda(t_0) + \int_{t_0}^{t} (t-\lambda)\,\frac{b}{a}\,\frac{\dot{\theta}}{\theta}\,dt.$$

The SAI and S&M models depart for the case of variable stress. In analogy to the variable temperature case, the SAI model assumes that the response for variable temperature as well as for variable stress can be expressed as

$$d\epsilon_x = \frac{\partial \epsilon_x}{\partial t}\,dt + \left[\frac{\partial \epsilon_x}{\partial \lambda}\,d\lambda + \frac{\partial \epsilon_x}{\partial \theta}\,d\theta + \frac{\partial \epsilon_x}{\partial \sigma_x}\,d\sigma_x\right]$$

$$= \frac{a\epsilon_x}{t-\lambda}\,dt + \left[\frac{-a\epsilon_x}{t-\lambda}\,d\lambda + b\epsilon_x\frac{d\theta}{\theta} + c\epsilon_x\frac{d\sigma_x}{\sigma_x}\right].$$

The sum of the terms in the bracket must be zero by creep strain continuity. Then the SAI pillar creep model for variable temperature and stress becomes

$$\epsilon_x = A[t - \lambda(t)]^a\,[\theta(t)]^b\,[\sigma_x(t)]^c \qquad \text{(A-4a)}$$

$$\dot{\epsilon}_x = a\,\epsilon_x/(t-\lambda) \qquad \text{(A-4b)}$$

$$\lambda(t) = \lambda_0 + \int_{t_0}^{t}\left(\frac{t-\lambda}{a}\right)\left[b\,\frac{\dot{\theta}}{\theta} + c\,\frac{\dot{\sigma}_x}{\sigma_x}\right]dt. \qquad \text{(A-4c)}$$

The analogous treatment of θ and σ_x in the SAI model is not present in the S&M model. The S&M model assumes that a change of stress (at constant temperature) occurring at τ produces a change of creep strain at $t \geq \tau$, according to

$$d\epsilon_x(t \geq \tau) = A(t-\tau)^a\theta_0^b d[\sigma_x(\tau)]^c$$

or

$$\epsilon_x(t \geq \tau) = \epsilon_x(\tau) + d\epsilon_x(t \geq \tau).$$

The generalization for variable stress and temperature results in the S&M pillar creep model,

$$\epsilon_x = A\int_{t_0}^{t}\left[\int_{\tau}^{t}\theta^{b/a}(u)du\right]^a \frac{\partial}{\partial\tau}[\sigma_x(\tau)]^c\,d\tau. \qquad \text{(A-5)}$$

It can be shown that the SAI and S&M pillar creep models of Eqs. (A-4) and (A-5) are identical for constant stress cases.* In addition, they converge to the same result for variable stress cases as time unfolds beyond the last stress change. The S&M model predicts infinite creep rate at stress jumps applied during creep, in contrast to the SAI model. Both models predict finite creep rate at temperature jumps applied during creep. Stress jump experiments would be required to select the most accurate model.

NUMERICAL CONSIDERATIONS

The steps to implement the SAI model numerically are:

1. Generalize the SAI pillar model for geometric invariance for application to arbitrary configurations.
2. Include the relations for stress relaxation due to creep strain.
3. Express the total model in appropriate difference form for inclusion in a time-explicit, finite-difference code.

In order to generalize the SAI pillar model [Eq. (A-4)], the pillar creep strain, ϵ_x, must be replaced by an equivalent deviatoric strain, $\sqrt{3}\,\langle e\rangle$, so that

$$\langle e\rangle \equiv \sqrt{\frac{1}{2}(e_{xx}^2 + e_{yy}^2 + e_{zz}^2) + e_{xy}^2 + e_{yz}^2 + e_{zx}^2}$$

where e_{ij} are the deviatoric strain components, and the pillar load, σ_x, must be replaced by an equivalent deviatoric stress, $\sqrt{3}\,\langle s\rangle$, so that

$$\langle s\rangle \equiv \sqrt{\frac{1}{2}(s_{xx}^2 + s_{yy}^2 + s_{zz}^2) + s_{xy}^2 + s_{yz}^2 + s_{zx}^2}$$

*when a constant value of σ_x is applied suddenly at t_0.

where s_{ij} are the deviatoric stress components. Assuming that creep is purely deviatoric, the invariant form of the SAI pillar model becomes

$$<\dot{e}^{cr}> = A[t - \lambda(t)]^a\,[\theta(t)]^b\,[<s(t)>]^c, \qquad \text{(A-6a)}$$

$$<\dot{e}^{cr}> = a<e^{cr}>/(t - \lambda). \qquad \text{(A-6b)}$$

$$\lambda(t) = \lambda_0 + \int_0^t \left(\frac{t-\lambda}{a}\right)\left[b\frac{\dot{\theta}}{\theta} + c\frac{<\dot{s}>}{<s>}\right] dt \qquad \text{(A-6c)}$$

where A is now a material constant that does not depend on the geometry. The superscript *cr* indicates that Eqs. (A-6) are for creep strain. These equations are useful only if θ and <s> are applied conditions. In particular, they do not handle cases of applied total strain. These latter cases correspond to stress relaxation due to the conversion of elastic strain into creep strain. Before addressing this effect, it is helpful to outline a numerical method, developed by Wilkins (Reference 3), used to relax stress by plastic flow. The extension of this method to creep flow can be derived by analogy.

The Wilkins approach involves the following steps. Compute deviatoric stress components from components of total deviatoric strain, assuming elastic theory. From Hooke's Law, the rate of change of deviatoric stress is directly proportional to the deviatoric strain rate,

$$\dot{s}^{ee}_{ij} = m\mu\dot{e}^{tot}_{ij} \qquad \text{(A-7a)}$$

where m = 1 when $i \neq j$ and m = 2 when i = j. μ is the elastic shear modulus. The computation of the deviatoric stress requires that Eq. (A-7a) be integrated,

$$s^{ee}_{ij}(t_n) = s_{ij}(t_o) + \dot{s}^{ee}_{ij}\Delta t \qquad \text{(A-7b)}$$

where $\Delta t = t_n - t_o$, t_n is new time, and t_o is old time. The stress ellipsoids before and after the computation of the new deviatoric stress in Eq. (A-7b) are shown schematically in Figure 4(a). These deviatoric stress components are called the equivalent-elastic deviatoric stress, $s^{ee}_{ij}(t_n)$, and are used to define a "trial" state of stress, $\sqrt{3}<s^{ee}(t_n)>$, which can be compared to the yield stress, $Y(t_n)$. If the trial state exceeds the yield surface defined by $Y(t_n)$, then all of the equivalent-elastic deviatoric stress components are reduced by the same factor,

$$\alpha = \frac{Y(t_n)}{\sqrt{3}\,<s^{ee}(t_n)>}. \qquad \text{(A-7c)}$$

Equation (A-7c) is a statement of the non-associative Prandtl-Reuss flow rule. The resulting deviatoric stress components and the corresponding plastic flow components are derived from the definition of total deviatoric strain rate as follows,

$$\text{let } \beta = \frac{1-\alpha}{\alpha\,\Delta t} \qquad \dot{e}^{tot}_{ij} = \dot{e}^{e}_{ij} + \dot{e}^{p}_{ij} \qquad \text{(A-8a)}$$

$$\dot{e}^{tot}_{ij} = \frac{\dot{s}^{ep}_{ij}}{2\mu} + \frac{\beta s^{ep}_{ij}(t_n)}{2\mu}$$

$$2\mu\dot{e}^{tot}_{ij} = \dot{s}^{ep}_{ij} + \beta s^{ep}_{ij}(t_n)$$

$$\dot{s}^{ep}_{ij} = \dot{s}^{ee}_{ij} - 2\mu\dot{e}^{p}_{ij}. \qquad \text{(A-8b)}$$

where β in the above equations is the constant of proportionality relating the rate of plastic strain to the instantaneous stress deviator in simple plastic theory.

Equation (A-8b) can be rearranged as follows,

$$\dot{s}^{ep}_{ij} = \dot{s}^{ee}_{ij} - 2\mu\dot{e}^{p}_{ij}. \qquad \text{(A-8c)}$$

In words, Eq. (A-8c) is

$$\begin{bmatrix}\text{Final}\\ \text{(elastic-plastic)}\\ \text{state of stress}\end{bmatrix} = \begin{bmatrix}\text{Trial}\\ \text{(equivalent-elastic)}\\ \text{state of stress}\end{bmatrix} - \begin{bmatrix}\text{Plastic}\\ \text{adjustment}\end{bmatrix} \qquad \text{(A-9)}$$

The elastic-plastic stress deviator, s^{ep}_{ij}, can be eliminated from Eq. (A-8c) by using Eq. (A-7c) in the following form,

$$\alpha = \frac{s^{ep}_{ij}(t_n)}{s^{ee}_{ij}(t_n)} \qquad \text{(A-10)}$$

Thus, Eq. (A-8c) becomes

$$\alpha s^{ee}_{ij} = s^{ee}_{ij} - 2\mu\dot{e}^{p}_{ij}\,dt$$

$$(1-\alpha)s^{ee}_{ij}(t_n) = 2\mu\dot{e}^{p}_{ij}dt. \qquad \text{(A-11a)}$$

It can also be shown that

$$(1-\alpha)<s^{ee}(t_n)> = 2\mu<\dot{e}^{p}>dt. \qquad \text{(A-11b)}$$

The elimination of $1-\alpha$ in Eqs. (A-11a) and (A-11b) results in the equations

$$\dot{e}^{p}_{ij} = <\dot{e}^{p}>\frac{s^{ee}_{ij}}{<s^{ee}>} \qquad \text{(A-12)}$$

which are equivalent to the assumption that plasticity shrinks the stress ellipsoid without changing its eccentricity

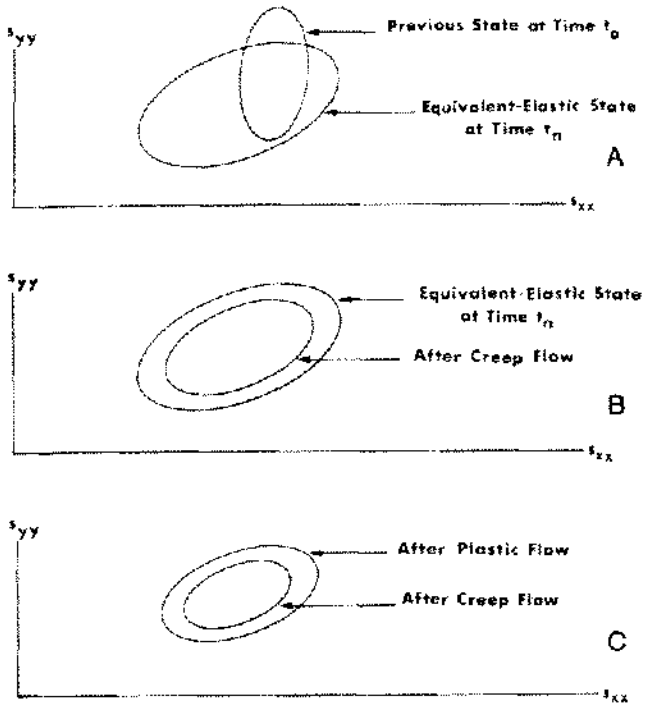

Figure 4. Update of stress deviators by elasti-plastic and creep adjustments. a) Stress deviator ellipsoid before and after elastic update. b) Plastic adjustment by the Pradtl-Reuss assumption (not essential to the creep model). c) Creep adjustment by the Prandtl-Reuss assumption (essential to the creep model).

or orientation. These remarks are illustrated in Figure 4(b). More general models of plasticity allow for rotations and distortions of the stress ellipsoid, and these are not precluded in the discussion that follows.

If we assume that creep strain relaxes the stress ellipsoid in the same non-associative manner described above, then the corresponding creep equations are

$$\dot{e}^{cr}_{ij} = <\dot{e}^{cr}> \frac{s^{ep}_{ij}}{<s^{ep}>} \tag{A-13}$$

where $s^{ep}_{ij}/<s^{ep}>$ is employed to account for general plastic response that does not necessarily obey Eqs. (A-12). This is consistent with the assumption that plastic relaxation of stresses occurs instantly, while creep relaxation requires time. Thus, the plastic adjustment is made first, followed by a creep adjustment based on the stresses that resulted from the plastic correction. Then, by direct analogy to the previous discussion [Eq. (A-8c)], the final deviatoric stresses, $s_{ij}(t_n)$, are

$$\begin{aligned} s_{ij}(t_n) &= s^{ep}_{ij}(t_n) - 2\mu\dot{e}^{cr}_{ij}dt \\ &= s^{ep}_{ij}(t_n)\left[1 - 2\mu<\dot{e}^{cr}>dt/<s^{ep}>\right] \end{aligned} \tag{A-14a}$$

$$\begin{aligned} <s(t_n)> &= <s^{ep}(t_n)> - 2\mu<\dot{e}^{cr}>dt \\ &= <s^{ep}(t_n)>\left[1 - 2\mu<\dot{e}^{cr}>dt/<s^{ep}>\right]. \end{aligned} \tag{A-14b}$$

The final adjustment due to creep is displayed in Figure 4(c).

If the heat generated by creep during the stress adjustment is either a) neglected, or b) not added, until after the adjustment, then we have enough independent equations to perform the stress-strain adjustment. However, the method must be centered properly to avoid systematic errors that can occur in difference equations. The method used by SAI is described next.

Previous expressions can be used to construct the difference equations,

$$\begin{aligned} <\dot{s}(t)> &\equiv \frac{<s(t_n)> - <s(t_o)>}{dt} \\ &= \frac{<s^{ep}(t_n)> - <s(t_o)>}{dt} - 2\mu<\dot{e}^{cr}> \\ &= \frac{<s^{ep}(t_n)> - <s(t_o)>}{dt} \\ &\quad - 2\mu aA(t_n-\lambda)^{a-1}[\theta(t_n)]^b\,[<s(t_n)>]^c \end{aligned} \tag{A-15}$$

$$\begin{aligned} \dot{\lambda}(t) &= [\lambda(t_n) - \lambda(t_o)]/dt \\ &= \frac{(t_n-\lambda)}{a}\left[\frac{b\dot{\theta}(t)/\theta(t_n) + \frac{c\left\{<s^{ep}(t_n)> - <s(t_o)>\right\}}{<s(t_n)>dt}}{}\right] \\ &\quad - 2\mu cA(t_n-\lambda)^a\,[\theta(t_n)]^b\,[<s(t_n)>]^{c-1}. \end{aligned} \tag{A-16}$$

Using the following conventions,

Knowns

t_o = old time
t_i = intermediate time ($t_o \le t_i \le t_n$)
t_h = half time $(t_o + t_n)/2$
t_n = new time
dt = full time step = $t_n - t_o$
$\lambda_o = \lambda(t_o)$
$s_o = <s(t_o)>$
$s^{ep}_n = <s^{ep}(t_n)>$
$R_o = \theta^b(t_o)$
$R_i = \theta^b(t_i)$
$R_n = \theta^b(t_n)$, $R_h = \theta^b(t_h)$
$\dot{R} = (R_n - R_o)/dt$

Unknowns

$s_i = <s(t_i)>$
$s_n = <s(t_n)>$
$\lambda_i = \lambda(t_i)$
$\lambda_n = \lambda(t_n)$

the difference equations can be expressed as

$$\dot{s}(t_i,\lambda_i,s_i,R_i) = \frac{s_n^{ep} - s_i}{dt} - 2\mu a A(t_i - \lambda_i)^{a-1} R_i s_i^a$$

$$\dot{\lambda}(t_i,\lambda_i,s_i,R_i) = \left(\frac{t_i - \lambda_i}{a}\right)\left[\frac{\dot{R}}{R_i} + \frac{c(s_n^{ep} - s_i)}{s_i dt}\right]$$

$$- 2\mu c A(t_i - \lambda_i)^a R_i s_i^{c-1}.$$

These equations can be solved by a fourth-order Runge Kutta scheme as described below. The fourth-order Runge Kutta method involves four successive estimates of s and λ. The first estimates are

$$\dot{s}_1 = \dot{s}(t_0,\lambda_0,s_0,R_0)$$
$$\dot{\lambda}_1 = \dot{\lambda}(t_0,\lambda_0,s_0,R_0)$$
$$s_1(t_h) = s_0 + \dot{s}_1\, dt/2$$
$$\lambda_1(t_h) = \lambda_0 + \dot{\lambda}_1\, dt/2.$$

The second estimates are

$$\dot{s}_2 = \dot{s}(t_h,\lambda_1,s_1,R_h)$$
$$\dot{\lambda}_2 = \dot{\lambda}(t_h,\lambda_1,s_1,R_h)$$
$$s_2(t_h) = s_0 + \dot{s}_2\, dt/2$$
$$\lambda_2(t_h) = \lambda_0 + \dot{\lambda}_2\, dt/2.$$

The third estimates are

$$\dot{s}_3 = \dot{s}(t_h,\lambda_2,s_2,R_h)$$
$$\dot{\lambda}_3 = \dot{\lambda}(t_h,\lambda_2,s_2,R_h)$$
$$s_3(t_n) = s_0 + \dot{s}_3\, dt$$
$$\lambda_3(t_n) = \lambda_0 + \dot{\lambda}_3\, dt.$$

The fourth estimates are

$$\dot{s}_4 = \dot{s}(t_n,\lambda_3,s_3,R_n)$$
$$\dot{\lambda}_4 = \dot{\lambda}(t_n,\lambda_3,s_3,R_n)$$
$$s_4(t_n) = s_0 + \dot{s}_4\, dt$$
$$\lambda_4(t_n) = \lambda_0 + \dot{\lambda}_4\, dt.$$

The final estimates are

$$s_n = s_0 + \frac{dt}{6}\left[\dot{s}_1 + 2\dot{s}_2 + 2\dot{s}_3 + \dot{s}_4\right]$$

$$\lambda_n = \lambda_0 + \frac{dt}{6}\left[\dot{\lambda}_1 + 2\dot{\lambda}_2 + 2\dot{\lambda}_3 + \dot{\lambda}_4\right]$$

where the errors in s and λ are estimated by

$$E_s = |(\dot{s}_3 - \dot{s}_2)/(\dot{s}_2 - \dot{s}_1)| \text{ if } \dot{s}_2 \neq \dot{s}_1$$
$$= 0 \text{ otherwise}$$
$$E_\lambda = |(\dot{\lambda}_3 - \dot{\lambda}_2)/(\dot{\lambda}_2 - \dot{\lambda}_1)| \text{ if } \dot{\lambda}_2 \neq \dot{\lambda}_1$$
$$= 0 \text{ otherwise.}$$

The SAI model used the criterion that E_s and E_λ could not exceed 2%. If this value was exceeded using a full time step, then the calculation was repeated with sub-time steps that reduced the error to 2% or less. Though the 2% criterion is frequently used in the Runge Kutta method, it is probably more conservative than is warranted for the Project Salt Vault simulation. The trade-off of accuracy versus computer costs was not assessed.

It should be emphasized that the present SAI creep model is based on limited data, applicable to salt repository conditions, and may not be valid under different conditions. The modeling method, however, is not constrained by the particular creep law that was selected. For example, the temperature dependency, θ^b, is a satisfactory description in the limited cases of the Lomenick experiments. The dependency, $\exp(-K/\theta)$ is equally satisfactory with respect to the Lomenick experiments and probably has a larger range of validity because of its agreement with dislocation theory (Reference 4). Either form can be handled with ease by the modeling method that has been presented. If necessary, the effects of dilatancy on creep rate may also be incorporated without difficulty.

RESULTS

So far, the only verification of the creep model comes from two-dimensional numerical simulations of PSV (Reference 5) using the explicit finite-difference code, STEALTH 2D (Reference 6). Room closure data comparisons between field measurements and results from simulations with and without the excavation sequence are shown in Figure 5. A full three-dimensional simulation is now underway.

ACKNOWLEDGEMENT

The work described in this paper was sponsored by the Office of Waste Isolation, Oak Ridge National Laboratory, Oak Ridge, Tennessee, USA.

REFERENCES

1. Bradshaw, R.L. and McClain, W.C. 1971. Project Salt Vault: A Demonstration of the Disposal of High-Activity Solidified Wastes in Underground Salt Mines. ORNL-4555, Oak Ridge National Laboratory, Oak Ridge, Tennessee.
2. Starfield, A.M. and McClain, W.C. 1973. Project Salt Vault: A Case Study in Rock Mechanics. Int. J. Rock Mech. Min. Sci. and Geomech. Abstr. 10: 641–657.

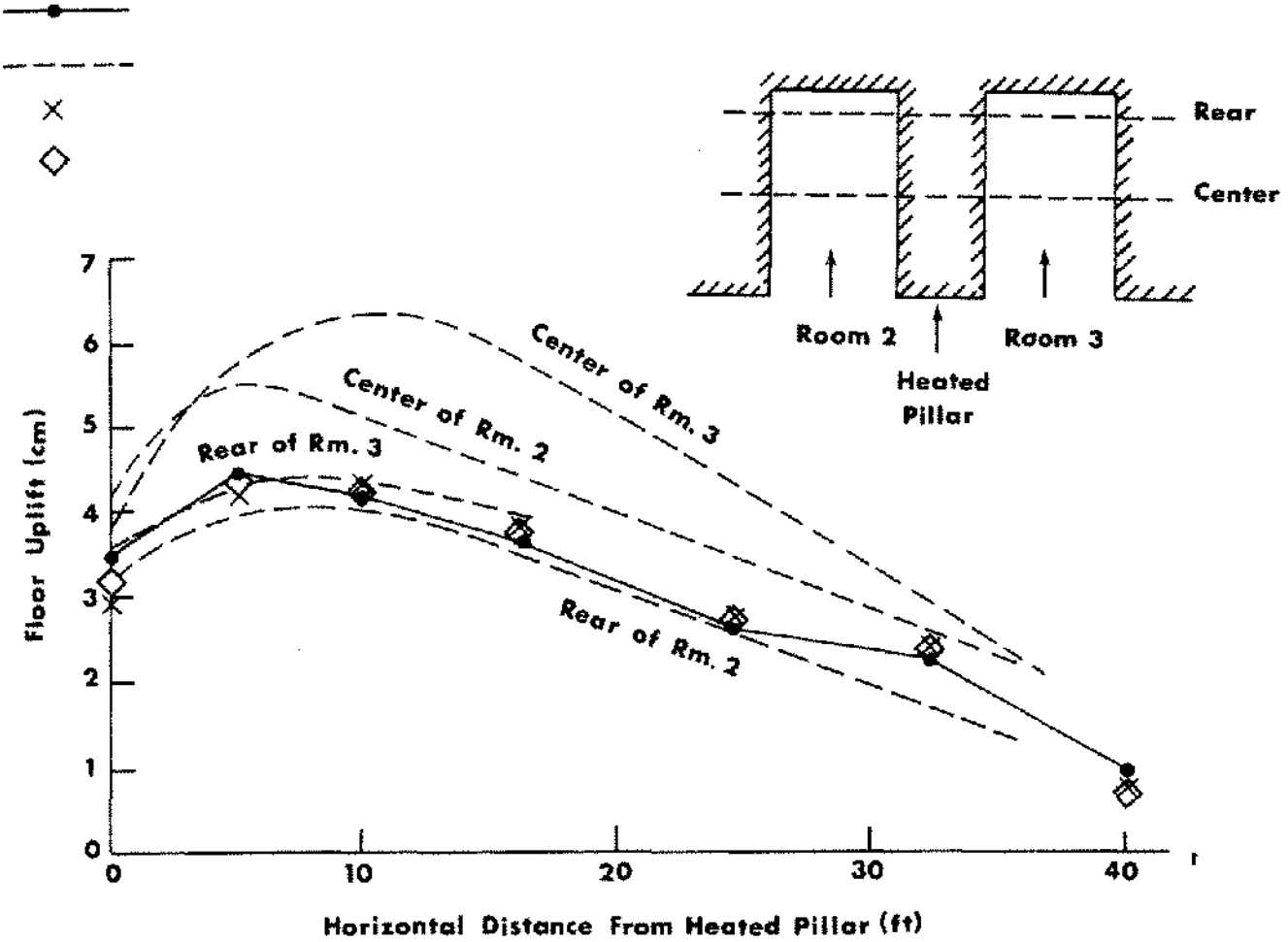

Figure 5. Floor uplift, standard days 1020 to 1501 (four-room simulation). Room 3 or 2 (two room simulation, solid line. ORNL-455 dashed line. Room 2 (sequential simulation), X line. Room 3 (sequential simulation) diamond line.

3. Wilkins, M.L. 1969. Calculation of Elastic-Plastic Flow. UCRL-7322, Rev. 1. Lawrence Radiation Laboratory, Livermore, California. January 24, 1969.

4. Heard, Hugh C. 1972. Steady-State Flow in Polycrystalline Halite at Pressure of 2 Kilobars. Flow and Fracture of Rocks. Geophysical Monograph Series 16.

5. Wahi, Krishan K., Maxwell, Donald E. and Hofmann, Ronald. 1978. A Two-Dimensional Simulation of the Thermomechanical Response of Project Salt Vault Including the Excavation Sequence. Y/OWI/SUB-78/16549/2 (SAI-FR-821-2), Science Applications, Inc., Oakland, California, March 1978. Final Report prepared for Office of Waste Isolation, Union Carbide Corporation, Oak Ridge, Tennessee.

6. Hofmann, Ronald and Gerber, Bence I. 1976. STEALTH, A Lagrange Explicit Finite-Difference Code for Solids, Structural, and Thermohydraulic Analysis. EPRI NP-260: 1–4. Science Applications, Inc., Oakland, California, August 1976. Prepared for Electric Power Research Institute, Palo Alto, California.